J Musculoskelet Neuronal Interact 2025; 25(4):392-406

Journal of Musculoskeletal and Neuronal Interactions JMNI

Original Article

Calvarial Bone Defects Heal Better in Short-Term Ovariectomized Rats Compared to Healthy Rats

Auden P. Balouch[1], Evan Marcet[1], Jasmine Bogle[1], Samantha J. Wojda[1], Seth W. Donahue[1]

[1]Department of Biomedical Engineering, University of Massachusetts Amherst, USA

Abstract

Objectives: Postmenopausal women develop estrogen deficiency which produces a pro-resorptive bone environment, leading to osteoporosis and increased fracture risk. Craniectomies are a common clinical procedure, especially in older populations, where calvarial bone is removed to relieve intracranial pressure (i.e., in the case of traumatic brain injury or stroke). Cranial reconstruction surgeries often result in failure due to infection or resorption of autograft material. Despite the need for calvarial bone graft alternatives for older patients, there is limited literature available on the effects of estrogen deficiency on skull bone metabolism and healing. **Methods**: The purpose of this work was to assess the effects of short-term ovariectomy (OVX) on calvarial bone properties and on the healing of 3.5 mm unilateral calvarial defects. **Results**: Surprisingly, the intact calvarial bone of OVX rats had higher bone volume, thickness, and number of remodeling cavities than intact calvaria of sham rats. Normalized measures of bone volume showed consistently more calvarial defect healing in OVX compared to sham rats at 4-, 8-, and 12-weeks post-surgery. **Conclusion**: These findings have implications for future investigations on therapies for treating calvarial bone defects in ovariectomy-induced osteoporotic rats.

Keywords: Bone Healing, Calvarial Defect, Ovariectomy, OVX, Short-Term OVX

Introduction

Menopause, which typically begins between 45 and 55 years of age, leads to estrogen deficiency that produces a pro-resorptive bone microenvironment, leading to osteoporosis and increased incidence of fractures[1–3]. Osteoporotic patients are also at greater risk of impaired healing of comminuted fractures and large bone defects that require surgical intervention[1,2]. It is estimated 40% of women will sustain an osteoporotic-related fracture in their lifetime[3,4]. It is well known that osteoporosis reduces bone mass, strength, and skeletal micro-architecture in long bones[1–4]. However, less is known about how osteoporosis affects the cranium and mandible. Craniectomies are performed clinically for several conditions including congenital anomalies, traumatic brain injuries (TBI), stroke, aneurysms, and cancer[5]. For the 1.5 million people in the US who sustain TBI annually, 2-14% of patients undergo emergent decompressive craniectomy to relieve intracranial pressure[5,6]. Calvarial bone is removed during craniectomy and stored sterilely until swelling has subsided, 1-3 months after the original surgery[5,6]. However, due to the prolonged storage time, survival of cellular material in banked autologous calvarial grafts is likely low, and 7-20% of reconstruction surgeries in adults result in failure due to resorption of the graft. An additional 7-10% of reconstructive surgeries fail due to infection. In these scenarios, a secondary reconstructive surgery is required using an alternative material[5]. The incidence of TBI is higher in people above 60 compared to younger adults[6]. Despite the need for calvarial bone graft replacements for older populations, there is limited literature available on the effects of estrogen deficiency on skull bone metabolism and healing.

Estrogen deficient ovariectomized (OVX) rats are the FDA recommended pre-clinical model for evaluating osteoporosis therapies in long bones[2,3], and the rat calvarial defect is a common model for the assessment of bone regeneration therapies[7–9]. Despite the common use of these

The authors have no conflict of interest.

Corresponding author: Auden P. Balouch, University of Massachusetts Amherst, Life Science Laboratories, 240 Thatcher Road, Amherst, MA 01003 USA
E-mail: abalouch@umass.edu

Edited by: G. Lyritis
Accepted 19 September 2025

combined models (i.e., calvarial defects in OVX rats)[10–20], impaired calvarial defect healing as a result of OVX has not been thoroughly studied, and the reports show conflicting results in untreated[11,13] and treated rats[10,13,20]. In a 3 mm calvarial defect created 8 weeks post-OVX, OVX rats had impaired bone healing of untreated defects compared to ovary-intact rats, based on radiographic signal intensity, 6 months after defect surgery[11]. Conversely, in a untreated 7 mm calvarial defect created 4 weeks post-OVX, there was a nonsignificant trend for higher bone volume within the defect space of OVX rats compared to rats receiving sham OVX[13]. Additionally, there was improved healing in OVX rats, compared to sham rats, that received an absorbable collagen sponge as treatment for the defect[13]. These conflicting reports demonstrate the need for a better understanding of the impact of estrogen deficiency on calvarial bone healing.

The purpose of this work was to compare the effects of OVX on tibial, mandibular, and calvarial bone properties. Additionally, the effects of OVX on calvarial bone defect healing was assessed longitudinally. It was hypothesized that OVX animals would have bone loss at all three skeletal locations and impaired calvarial bone defect healing compared to healthy animals because of the pro-resorptive microenvironment induced by estrogen deficiency. The findings from this study increase our understanding of the effects of the OVX on bone properties at multiple skeletal sites, including the calvaria. The results also provide a better understanding of how calvarial bone defects heal under osteoporotic conditions.

Materials and Methods

Animal Model. A study timeline is presented in Figure 1. Twelve-week-old female Sprague Dawley rats (230-330 g) underwent ovariectomy (n=9) and sham (n=9) surgeries at the vendor (Charles River Laboratories). Post-surgery, animals were group housed (standard 12:12 light:dark, 24°C) with wood shavings (bedding), cardboard tunnel and nesting and standard food and water provided *ad libitum*. Two weeks post-surgery, all animals received a 3.5 mm unilateral calvarial bone defect and were left untreated. Prior to surgery, and at 4-, 8-, and 12-weeks post-surgery, calvarial bones were scanned with microcomputed tomography (μCT) to assess defect healing and the effects of OVX on the bone properties of the contralateral, intact calvaria. The proximal tibia was scanned at 3- and 14-weeks post-OVX surgery since this site is well known to demonstrate bone loss[14,21,22]. Additionally, the mandible was scanned at 14-weeks post-OVX surgery to assess the possible effects of OVX on mandibular bone properties. All μCT image processing and analyses were performed blinded from experimental group. Twelve weeks after calvarial defect surgery, rats were anesthetized via isoflurane inhalation (2.8%) and euthanized via intra-cardiac exsanguination. The uteri were harvested and weighed for the verification of the OVX surgery efficacy.

Calvarial Defect Surgery. At 2 weeks post-OVX and sham procedures, rats underwent surgery to create a 3.5 mm unilateral calvarial defect in the parietal bone following established protocols[7]. Surgery orders were randomized and performed with surgeon blinded to experimental group (OVX or sham). Rats were anesthetized, to effect, via isoflurane inhalation (2.2-2.8%). Animals received buprenorphine SR (0.65 mg/kg) subcutaneously 30 minutes prior to surgery for pain management, cefazolin (20 mg/kg) as a prophylactic antibiotic, and sterile saline (5 mL/kg) for loss of fluids. Under anesthesia, the incision site (i.e., from bridge of nose to the back of head) was shaved and disinfected with isopropyl alcohol and chlorohexidine. A midline incision 1-2 cm in length was made at the calvaria through the skin and underlying periosteum along the sagittal suture. The periosteum was laterally retracted from the defect site using an elevator and Brown-Adson forceps. Under irrigation, a trephine bur operating at 1500 RMP was used to create a 3.5 mm diameter unilateral circular defect in the left parietal bone, centered between the coronal and lambdoid sutures. Caution was taken not to damage the underlying dura mater. The defect was completed by removing the segmented bone from the defect area using a surgical elevator. Sterile saline irrigation and gauze were used throughout the procedure to manage bleeding and prevent thermal injury from drilling. The periosteum and skin were separately sutured closed using 4-0 monofilament absorbable sutures. Wound clip staples were placed over the incision and removed 10 days post-op. The wound site was cleaned with hydrogen peroxide and animals were left to recover on a heating pad until fully awake. Animals were monitored daily for signs of distress and evidence of wound problems for 7 days following surgery. The body weight of rats was recorded every two weeks upon arrival until euthanasia.

Micro-Computed Tomography (μCT).

μCT of proximal tibial metaphysis. At 3- and 14-weeks post-OVX, the proximal tibial metaphysis was scanned *in vivo* and *ex vivo*, respectively, with Skyscan 1276 (Bruker Optics, USA) μCT system. Scans were taken with voxel size of 18 μm[23], voltage of 100 kV, current of 200 μA, exposure of 350 ms, and a rotation of 180° with a 0.50° step to assess trabecular bone loss over the 14-week post-OVX period[2]. Scans were processed to remove any ring, motion, or other artifacts including beam hardening reduction, Gaussian filtration, and misalignment compensation (NRecon v.1.7.4). A cylindrical volume of interest (VOI), 1.6 mm in height, starting 2 mm distal to the growth plate (Figure 2) was used to evaluate trabecular bone (CTAnalyser v.1.17). The VOI diameter (1.95 ± 0.06 mm) was variable between samples to include as much trabecular bone as possible within the cortex of the tibial metaphysis. Bone volume fraction (BV/TV), trabecular thickness (Tb.Th), number (Tb.N), separation (Tb.Sp), and tissue mineral density (TMD) were quantified. An adaptive threshold (within range of 0.39-0.61 gHA/

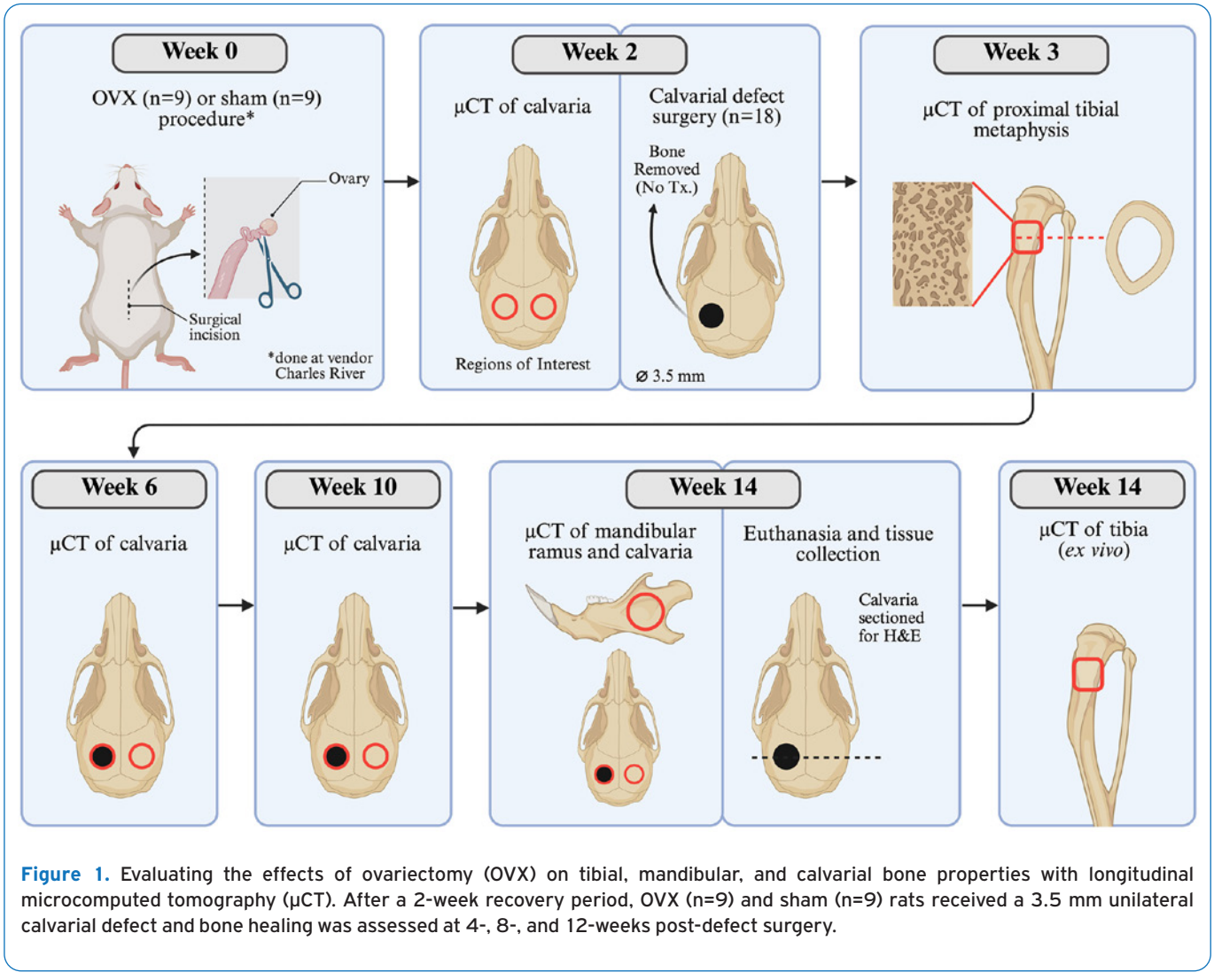

Figure 1. Evaluating the effects of ovariectomy (OVX) on tibial, mandibular, and calvarial bone properties with longitudinal microcomputed tomography (µCT). After a 2-week recovery period, OVX (n=9) and sham (n=9) rats received a 3.5 mm unilateral calvarial defect and bone healing was assessed at 4-, 8-, and 12-weeks post-defect surgery.

cm^3 based on neighboring pixels) was used to differentiate mature mineralized trabecular bone from other tissues. Additionally, cortical area (Ct.Ar), average cortical thickness (Ct.Th), periosteal perimeter (Ps.Pm) and endocortical perimeter (En.Pm) were quantified in the proximal tibial metaphysis. A global threshold of 0.65 gHA/cm^3 was used to differentiate mature mineralized cortical bone from other tissues[24]. A 2D cross section 2.8 mm distal to the growth plate, mid-height of the trabecular VOI, was used to trace the periosteal and endocortical perimeters (BIOQUANT OSTEO v.12.1.60); cortical thickness was automated to measure every 1 µm between drawn perimeters and an average value is reported.

µCT of ramus of mandible. At 14 weeks post-OVX, mandibles were scanned *in vivo* with a voxel size of 40 µm, voltage of 60 kV, current of 125 µA, exposure of 539 ms, and a rotation of 360° with a 0.80° step. Scans were processed to remove any ring, motion, or other artifacts including beam hardening reduction, Gaussian filtration, and misalignment compensation. To quantify mandibular bone volume (BV) and TMD, a 5.0 mm diameter cylindrical VOI overlaid the ramus of the mandible. Tissues > 0.65 gHA/cm^3 were considered mature mineralized bone[24]. A 5.0 mm VOI was used for the mandible given this is a common size and site for mandibular bone defects[25–27]. The thickness of the cylindrical VOI was variable to span the thickness of each rat's mandible.

µCT of intact calvaria. At 2- and 14-weeks post-OVX, *in vivo* µCT scans were taken of the calvaria with the same scanning parameters and post-processing methods as mandibular scans. To quantify native skull bone properties, a 3.5 mm diameter cylindrical VOI overlaid on the right parietal bone of the calvaria, contralateral to the bone defect space, and spanned the height of rats' native skull. Tissues

>0.65 gHA/cm^3 were considered mature mineralized bone[24]. BV and TMD were quantified.

Transverse plane µCT images of the intact calvaria, midway between the coronal and lambdoid sutures, were used to evaluate bone density gradients produced by bone modeling activity. Transverse images prior to and 12-weeks post-defect surgery were color coded based on tissue density in intervals of 0.10 gHA/cm^3, ranging from 0.25 to 1.15 gHA/cm^3. Intervals above 0.65 gHA/cm^3 were considered mature mineralized bone[24] and intervals below 0.65 gHA/cm^3 were considered under-mineralized bone. The total area of remodeling pores, the thicknesses of the mature mineralized skull, and the thickness of under-mineralized bone on the superior and inferior sides of the calvaria, spanning from the sagittal suture to the parietal ridge were quantified.

µCT of calvarial defect space. Prior to calvarial defect surgery as well as 4-, 8-, and 12-weeks post-defect surgery, *in vivo* µCT scans were taken of the calvaria capturing the bone defect space. Scans were taken with the same scanning parameters and post-processing methods as mandibular scans. To assess bone regeneration in the defects, a 3.5 mm diameter cylindrical VOI overlaid the defect space in frontal plane images to quantify BV and TMD of new tissues. Data were normalized to measures of the defect space prior to defect creation (week 2, Figure 1); reported as % bone volume filled and % TMD, respectively. Percent of defect area filled with bone (% bone area filled) was calculated as the percent area coverage of the defect space with new mineralized bone tissue at week 12. Tissues > 0.65 gHA/cm^3 were considered mature mineralized bone[24]. The height of the cylindrical VOI was variable between animals to span the entire height of each animal's native skull, capturing all new tissues within the defect space at each time point. Scans from each week were aligned with the pre-surgery longitudinal scans (DataViewer v.1.5.6) for consistent VOI placement. Images were registered by aligning the base image (earliest post-defect time point, week 4 post-surgery) with the defect space parallel to the coronal plane. This is done by adjusting all three planes (coronal, sagittal, and transverse) to align well with overlaying anatomical plane axes. Next, longitudinal scans are projected over base scans and aligned in all three planes (using both rotation and translation of the image dataset) to align with base scans. In each of the coronal, sagittal, and transverse planes, the image dataset is translated and rotated for alignment by checking multiple bony landmarks are aligned with base scans. This procedure ensures consistent and reproducible alignment of VOIs over the calvarial defect space of the same animal, longitudinally.

Histology: Following euthanization, the calvaria was removed, fixed in 10% formalin for 72 hours, and stored in 70% ethanol. Samples were decalcified, embedded in paraffin wax, and 5 µm thick sections were cut medio-laterally intersecting the approximate center of the defect space, and stained with Hematoxylin & Eosin (H&E). Slides were evaluated at 100x magnification using a Zeiss SteREO Discovery.V20 (Carl Zeiss Inc., Germany) light microscope. Within the defect space, the presence of bone, fat, dense connective tissue, loose connective tissue, blood vessels, and blood clots were graded on a scale of 0-3. A grade 0 indicates the absence of that tissue within the defect space, whereas a grade 3 indicates a high abundance relative to all samples. The intact calvaria, contralateral to the defect space, were assessed for bone remodeling activity, where remodeling spaces within the skull between the sagittal suture and parietal ridge were traced and the sum of remodeling cavity areas is reported. All histological analyses were performed blinded from experimental group.

Statistical Analysis

All µCT data fit a normal distribution (Shapiro-Wilk test, p>0.199). Histology grading data did not fit a normal distribution (Shapiro-Wilk test, p≤0.0114), included in Figure S1. For comparison of body and uteri weights and µCT data between OVX and sham rats at a single time point, an unpaired t-test was used. Longitudinal bone volume and TMD were normalized to each respective animals' measure at week 2, prior to defect creation. For comparison of longitudinal µCT data (i.e., % bone volume filled and % TMD), a repeated measures mixed model was used with Tukey post hoc pairwise comparisons; time and treatment group served as fixed effects and individual animals served as a random effect. Variables effect size on % bone volume filled and % TMD is reported as Cohens d, with 95% CIs, included in Table S1. A nonparametric Mann-Whitney test was used for comparison histology scores between OVX and sham rats. For all parametric analyses, data are presented as mean ± SE, or alternatively, group medians are reported. A p<0.05 was considered statistically significant (performed in JMP Pro v.1.17). No data were excluded from µCT and histological analyses (n=9 per group). Preliminary µCT was used to predict high statistical power (82%) to detect a 50% difference in bone volume of OVX compared to sham calvarial defects, with a sample size of ≥ 8 animals per experimental group.

Results

Animals. No animals exhibited signs of illness or infection post-surgery. The efficacy of OVX surgery and onset of osteoporosis were verified by increased body weight, decreased uterus weight, and tibial trabecular bone loss in OVX compared to sham animals at 14-weeks post-OVX. At euthanasia, the body weight of OVX rats was 131% the weight of sham rats (p<0.0001) and dry uterus weight was 23% of sham (p<0.0001).

Proximal Tibial Metaphysis. At 14 weeks post-OVX, OVX rats had decreased trabecular bone volume fraction (p=0.0006), number (p=0.0004), and TMD (p=0.0067); and increased trabecular separation (p=0.0004) in the proximal tibial metaphysis compared to sham rats (Figure

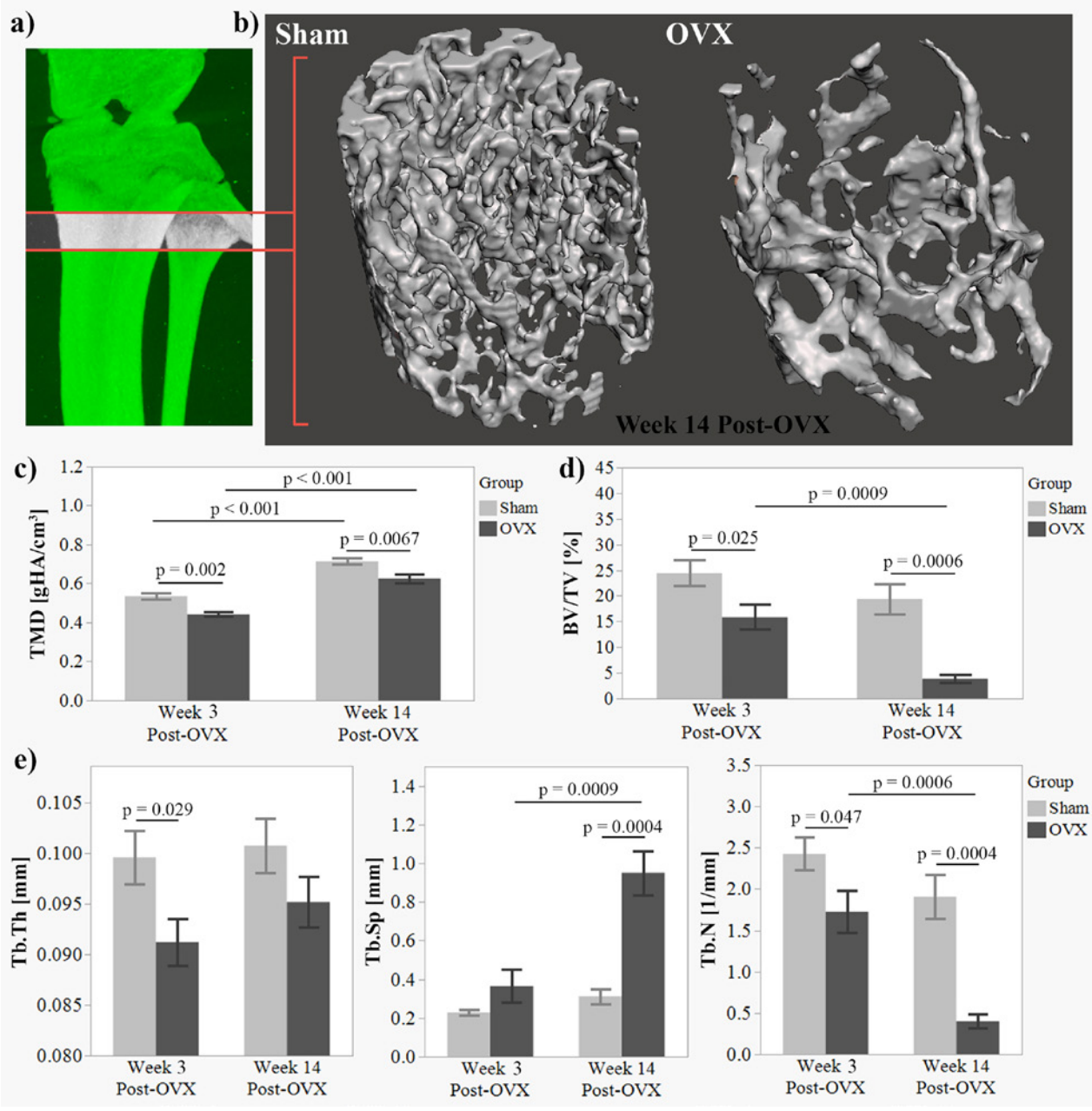

Figure 2. μCT results of trabecular bone of the proximal tibial metaphysis at 3- and 14-weeks post-OVX. a) Region from which cylindrical VOI of trabecular bone was obtained for μCT analysis, b) Representative OVX and sham 3D models of VOI, c) Tissue mineral density (TMD, gHA/cm^3), d) bone volume fraction (BV/TV, %), e) trabecular thickness (Tb.Th, mm), separation (Tb.Sp, mm), and number (Tb.N, 1/mm) in VOI. All graphs are mean ± SE.

2). Conversely, by 14 weeks post-OVX, OVX rats had increased cortical area (p=0.019), thickness (p=0.042), and periosteal (p=0.007) and endocortical perimeters (p=0.013) in the proximal tibial metaphysis compared to sham rats (Figure 3).

Ramus of the Mandible. At 14 weeks post-OVX, OVX and sham rats had similar bone volume (p=0.95; 4.71 ± 0.25 mm^3 and 4.73 ± 0.13 mm^3, respectively) and tissue mineral density (p=0.106; 0.88 ± 0.01 gHA/cm^3 and 0.91 ± 0.01 gHA/cm^3, respectively) in the ramus of the mandible.

Intact Calvaria. The intact calvaria showed increased BV in OVX rats compared to sham at 14 weeks (p=0.017)

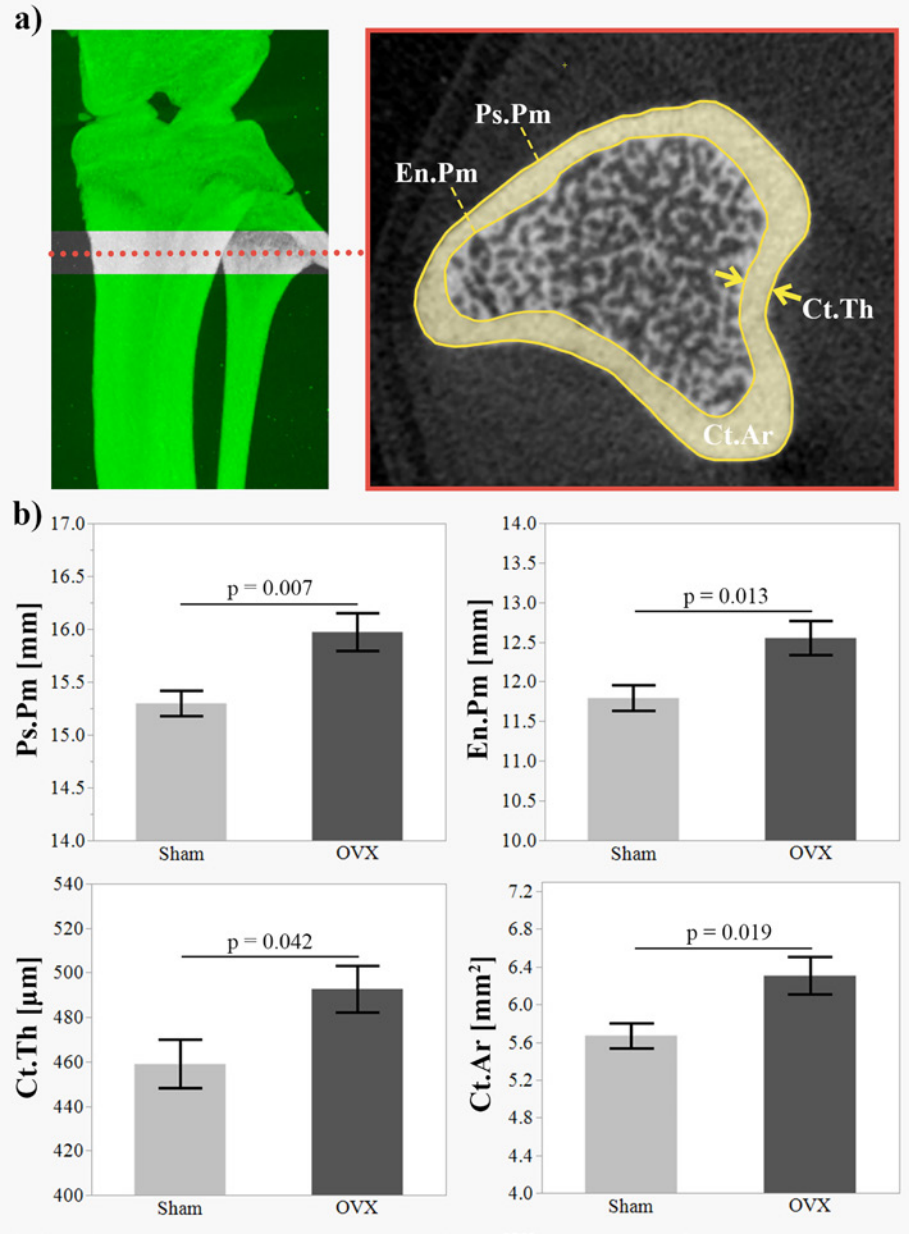

Figure 3. µCT results of cortical bone of the proximal tibial metaphysis at 14-weeks post-OVX. a) Location of 2D cross-section for µCT analysis and representative measures (Ps.Pm, periosteal perimeter; En.Pm, endocortical perimeter; Ct.Ar, cortical area; Ct.Th, cortical thickness, b) Length of periosteal perimeter (Ps.Pm, mm), length of endocortical perimeter (En.Pm, mm), average cortical thickness (Ct.Th, µm), and cortical area (Ct.Ar, mm^2). All graphs are mean ± SE.

post-OVX, but not at 2 weeks post-OVX (p=0.22) (Figure 4b). Conversely, the TMD of OVX rats was lower than sham at 14 weeks post-OVX (Figure 4c). Transverse µCT images colorized by tissue mineral density (Figure 4d) showed increased remodeling activity in OVX rats, with larger total area of remodeling spaces in the calvaria at 2 weeks (p=0.069) and 14 weeks (p=0.039) post-OVX (Figure 4e). Similarly, histological analysis showed OVX rats had a higher (p=0.019) total area of remodeling spaces than sham rats at 14 weeks post-OVX (Figure 5).

Additionally, based on colorized transverse µCT images, OVX rats had increased calvarial thickness compared to sham at 2 weeks and 14 weeks post-OVX (Figure 4f). The thickness of under-mineralized bone on the inferior side

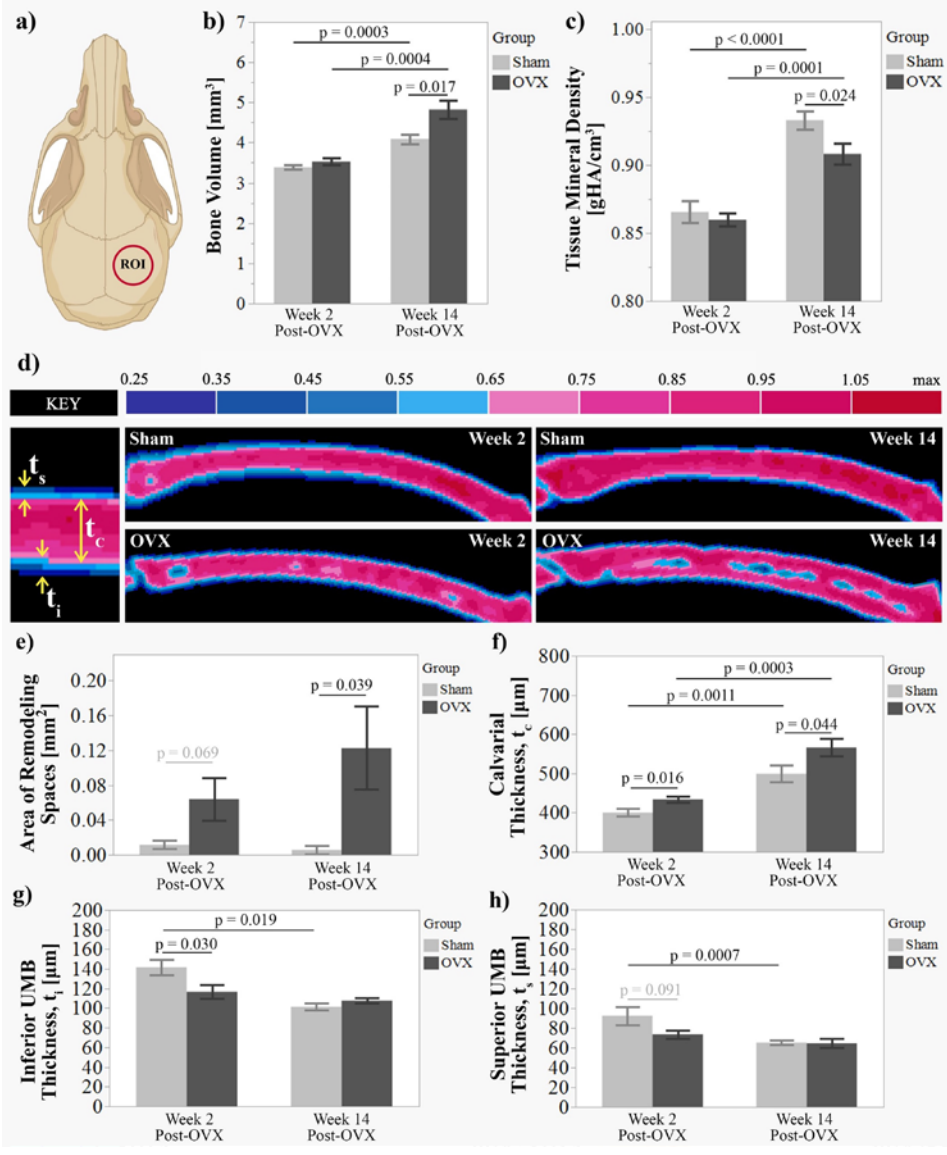

Figure 4. µCT results of intact calvaria at 2- and 14-weeks post-OVX. a) Location of region of interest (ROI) for µCT analysis of the intact calvaria, b) Bone volume and c) tissue mineral density in ROI, d) Representative measures (t_c, calvaria thickness; t_i, inferior thickness of under-mineralized bone; t_s, superior thickness of under mineralized bone) and representative OVX and sham density-based colorized µCT transverse images including under-mineralized bone (blues) and mature mineralized bone (pinks) above the set threshold (0.65 gHA/cm^3), e) Total area of remodeling spaces (under-mineralized areas within calvaria, mm^2), f) calvarial thickness (t_c; of mature mineralized bone, µm), and thickness of under-mineralized bone (UMB) on the g) inferior/dura mater surface (t_i, µm) and h) superior/periosteal surface (t_s, µm). All graphs are mean ± SE.

of the skull was greater (p<0.0001) than the thickness of under-mineralized bone on the superior surface of skull in all animals. At 2 weeks post-OVX, sham rats had a trend for larger (p=0.09) under-mineralized bone thickness on the superior surface (Figure 4g) than OVX rats, and a larger (p=0.03) thickness on the inferior surface (Figure 4h). Thickness of under-mineralized bone in sham rats decreased on both the superior and inferior bone surfaces while no changes were seen in OVX rats over time. There were no differences in superior (p=0.91) and inferior (p=0.17) thicknesses between OVX and sham rats 14 weeks post-OVX.

Calvarial Defect Space. At 4-, 8-, and 12-weeks post-defect surgery, there was more bone regeneration in OVX

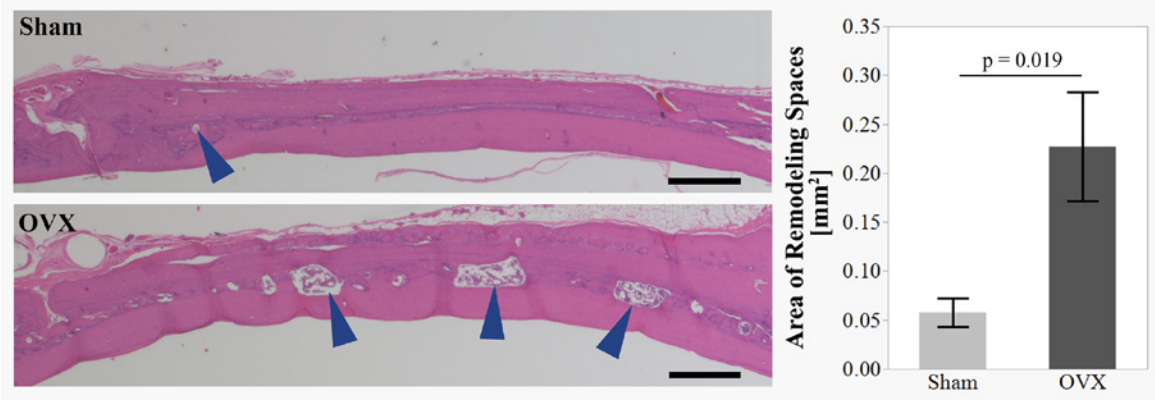

Figure 5. a) Representative stitched H&E images (scale bar = 500 µm) of remodeling spaces (blue arrows) in the intact calvaria of OVX and sham rats, b) Total area of remodeling spaces in intact calvaria (mm^2). Mean ± SE.

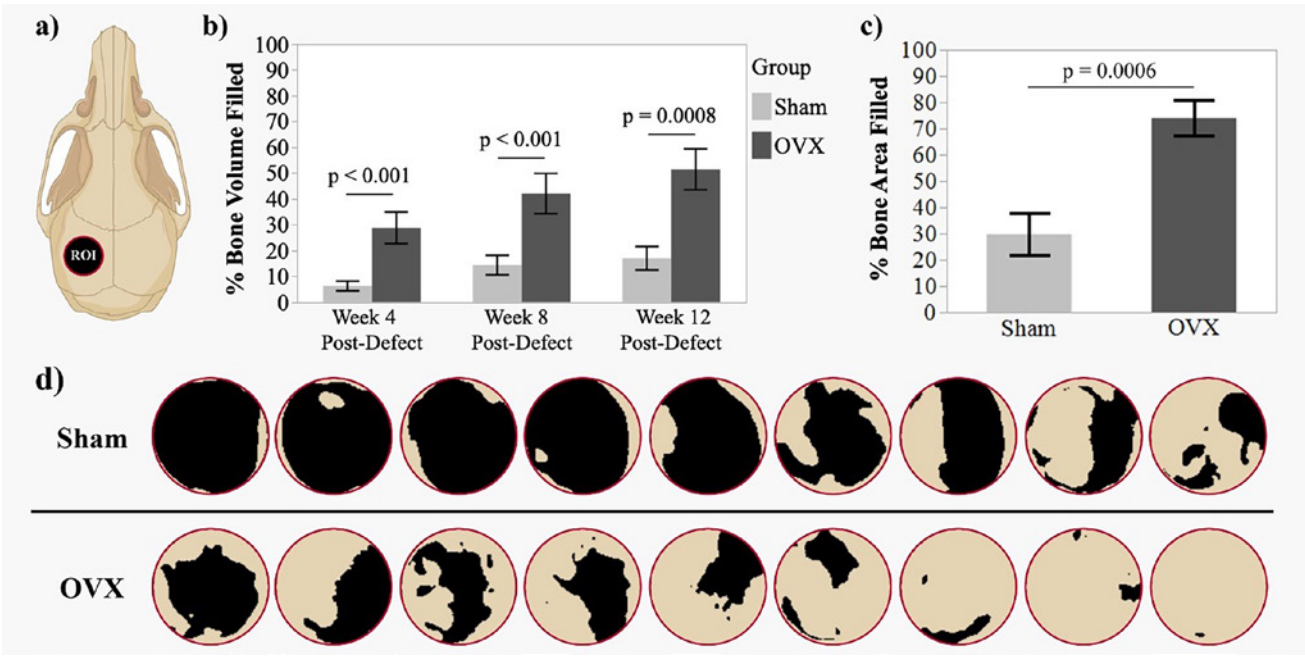

Figure 6. a) Location of ROI overlaying calvarial bone defect space to quantify bone healing with longitudinal µCT analysis, b) Percent bone volume filled at 4-, 8-, and 12-weeks post-defect surgery, relative to week 0 (pre-defect surgery), c) Percent bone area filled and d) 2D frontal plane images of % bone area filled of all samples, 12 weeks post-defect surgery. Tan represents mature bone tissue (>0.65 gHA/cm^3). All graphs are mean ± SE.

rats compared to sham rats ($p<0.008$, Figure 6b). Both fixed effects, time ($p<0.001$, $d>0.35$) and experimental group ($p=0.0025$, $d=1.63$), and the random effect of animal specificity ($p=0.0064$) were significant predictors of % bone volume in the defect space; but not the interaction of group x time ($p=0.585$, $d>0.15$). OVX rats also had a higher area of the defect space filled with mature mineralized bone (% bone area filled) at 12 weeks post-surgery ($p=0.0006$,

Figures 6c, 6d). The % TMD of the new bone in the defects was not dependent on experimental group (p=0.789, d=0.55). However, % TMD of both groups increased over time (p<0.0001, d>0.89) at similar rates (time x group, p=0.897, d>0.02). Additionally, the random effect of animal specificity (p=0.0125) was a predictor of TMD outcome. Pairwise effect sizes CIs (Cohen's d ±95%) on % bone volume filled and % TMD are reported in Table S1. Similar differences in new bone growth between OVX and sham was verified with histology samples of the defect space; group medians are reported with p-values. OVX rats had a trend for higher average grading for the presence of new bone tissue (sham 1.5, OVX 3; p=0.09). There were no differences between OVX and sham histology for the grading of other tissue types present in the defect space, including dense connective tissue (sham 2, OVX 1.5; p=0.11), loose connective tissue (sham 1, OVX 1; p=0.54), fat (sham 1, OVX 0.5; p=1), blood vessels (sham 2.5, OVX 2; p=0.9), and blood clots (sham 1.5, OVX 2; p=0.9).

Discussion

The calvarial defect model is used in research to assess bone healing under estrogen deficiency-induced osteoporotic conditions[15,17–19]. However, there is limited literature comparing bone healing of untreated calvarial defects between healthy and OVX rats[11,13], and of that literature, discrepancies in bone healing outcomes exist. Therefore, a better understanding of the effect of estrogen deficiency on bone properties of intact calvarial bones and the healing of calvarial bone defects is needed to improve the use of these combined models for assessing therapies to promote calvarial bone regeneration under osteoporotic conditions. We hypothesized that OVX rats would have impaired bone healing in the calvarial defect and bone loss at all skeletal sites (i.e., intact calvaria, ramus of the mandible, and proximal tibial metaphysis). However, at 14 weeks post-OVX, the effects of OVX on bone properties varied between skeletal locations, and there was enhanced bone healing in the calvarial defect space in OVX compared to sham rats.

This study demonstrated the effect of estrogen deficiency on bone properties was dependent on skeletal site and bone type. OVX rats had decreased trabecular bone volume fraction, with a concomitant increase in cortical bone thickness and area in the tibia, relative to sham rats. Additionally, the intact calvaria, contralateral to the defect space, of OVX rats had increased thickness and bone volume compared to sham rats. No bone loss or gain was observed in the mandible. In the trabeculae of the proximal tibial metaphysis, bone volume fraction was less in OVX rats compared to sham as early as 3 weeks post-OVX, with a significant decrease by 14 weeks post-OVX, as expected and consistent with previous literature[2,21,28,29]. Trabecular separation and number significantly increased and decreased, respectively, in OVX rats compared to sham rats at 14 weeks post-OVX. While trabecular thickness was lower in OVX rats compared to sham at 3 weeks post-OVX, there was a trend for increased trabecular thickness in OVX rats over the course of the study. This was likely due to complete resorption of thinner trabecular struts over the evaluation period. Conversely, in the cortical bone of the proximal tibial metaphysis, OVX rats had increased cortical area and cortical thickness. Increased bone modeling activity was evident by increased periosteal perimeters resulting from increased bone formation and increased endocortical perimeters resulting from increased bone resorption in OVX rats, similar to previous reports[28,30,31]. Interestingly, there were no differences in the bone properties of the mandible in OVX rats compared to sham. These results align with previous studies investigating site-specific bone characteristics in estrogen deficient conditions, where decreased femoral trabecular BV/TV was observed in OVX rats but no change in mandibular BV, compared to sham rats[32]. Similarly, there was no difference in mandibular basal bone microarchitecture between pre- and post-menopausal estrogen deficient women[33]. In the intact calvaria, along with increased bone volume, increased formation and resorption activity was observed in OVX rats compared to sham, evident by increased skull thickness and area of remodeling spaces, respectively, at 14 weeks post-OVX. Although increased bone volume was observed in the intact calvaria of OVX rats, overall bone quality may be compromised given the decreased TMD and increased cortical porosity in response to OVX-induced estrogen deficiency; similar to the changes observed in femoral cortical bone of OVX rats[28]. Increased BV in the calvaria is likely attributed to the site-specific increase in bone formation activity post-OVX, exceeding rapid bone resorption. Previous comparison of calvarial tissue pre- and post-OVX has shown increased mean bone formation rate, where no change was observed in the femur, and increased osteoclast surface at both sites post-OVX[34].

Observations of increased calvarial and tibial cortical bone in OVX rats are consistent with reports that estrogen acts to inhibit periosteal modeling (in formation mode) as young girls reach puberty and the inhibition of modeling is released when women go through menopause, leading to an increase in bone diameter[35]. Previous research has shown temporal increases in systemic markers of bone turnover (i.e., TRAP, P1NP, CTX, DPD), inflammation (i.e., TNF-a, IL-6), and α and β estrogen receptors (ER) early after OVX compared to sham animals[36–40]. However, literature in longitudinal site- and bone-type specific quantification is limited. Systemic serum markers of bone remodeling activity would not capture variability in expression by skeletal site or bone type. One study has demonstrated local histomorphology staining of OVX sheep metatarsal diaphysis had increased intracortical bone turnover compared to sham animals at 6-9 months, but not 1-3 or at 12 months post-OVX. Additionally, despite no differences in cortical thickness or area quantified by μCT, OVX had lower stiffness and yield strength under compressive testing[41]. One mechanism contributing to

increased modeling could be related to ERα and ERβ on bone cells, where ERα is the predominant isoform in cortical bone and ERβ is the predominant isoform in trabecular bone[42,43]. ERα knockout (ERαKO) mice and osteoblast-specific ERαKO mice have shown decreased cortical bone mineral density and increased trabecular bone mineral density, suggesting ERα is responsible for maintaining optimal periosteal bone formation through osteoblasts progenitors[43]. In contrast, ERβKO mice have shown increased cortical and trabecular bone mineral density[43]. Additionally, it has been reported that ERβ modulates ERα action in tissues where they are coexpressed (i.e., bone)[44] and the differential distribution of ERα and ERβ may play a role in site-specific variations in estrogen responsiveness[42]. The interaction of ERα and ERβ adds complexity to understanding the heterogeneous responses to estrogen deficiency within the skeleton, and further research is needed to better define the roles of ERα and ERβ in bone healing under estrogen deficient conditions. Bone microarchitecture, local formation markers, resorption markers, and local ERα and ERβ expression should be quantified longitudinally at different local bone sites (with distinct trabecular and cortical areas) to better understand this dynamic system in short-term OVX animals. A limitation of the current work is the use of young rats compared to middle aged (i.e., skeletally mature) rats, where young rats have increased trabecular remodeling in response to OVX[14,22,45,46], potentially contributing to OVX-induced changes in bone properties observed here. Animal age should be an important consideration for future studies wanting to represent the clinical scenario of estrogen deficiency in skeletally mature patients.

Surprisingly, OVX rats demonstrated superior healing of untreated 3.5 mm calvarial bone defects compared to healthy rats, with consistently higher % bone volume filled over time and a higher % defect area filled at 12 weeks post-defect surgery. We are 95% confident the experimental group had a large effect on % bone volume filled outcome (d=1.63, CI= [1.0, 2.25]). As previously discussed, the early effect of estrogen deficiency on bone modeling was evident in the intact calvaria, where OVX rats had increased bone volume and calvarial thickness compared to sham. In long bones, a temporal relationship between OVX and bone remodeling activity has been observed, where markers for bone formation and resorption were maximally elevated in the first 30 days following OVX, compared to sham rats, in the proximal tibial metaphysis[21], vertebrae[47], and femoral neck[46]. Calvarial defect creation during this early period of increased remodeling activity may be contributing to increased calvarial healing in OVX rats. Calvarial defects were created 2 weeks post-OVX and bone healing was evaluated at 4-, 8-, and 12-weeks post-defect surgery which varies from the previous studies of calvarial bone healing in OVX rats[10,11,13,20]. Calvarial healing in this study is consistent with the previous observation of a trend for higher bone volume in OVX rats with a 7 mm defect, 4 weeks post-surgery[13], as well as OVX rats treated with an absorbable collagen sponge[13] or a poly(lactic-co-glycolic acid) scaffold, 16 weeks post-OVX[20]. However, they conflict with another study which showed impaired bone healing in OVX rats that received a 3 mm defect, evaluated 6 months post-surgery[11]. Impaired healing was also found in OVX rats treated with a bovine bone graft at 4[10] and 8 weeks post-OVX[12]. It's possible the outcome of OVX healing is dependent on the timing of ovariectomy in relation to calvarial defect creation. Similar observations have been made in other native bone sites, with various microarchitectural changes dependent on the evaluation time point post-OVX[14,21,48–52]. Previous studies are difficult to directly compare due to differences in variability in animal strains, ages, different sized defects, and timing between OVX and calvarial defect surgery, all of which could contribute to healing outcome. Estrogen deficiency may cause an initial temporary increase in calvarial bone formation modeling that is later surpassed by resorptive modeling. This would result in improved bone deposition near the onset of estrogen deficiency, but impaired bone healing in longer term studies[11]. This temporal increase in parietal BV and thickness could affect calvarial healing; thus, μCT analyses have been normalized to animals' respective measures pre-defect. A limitation of the current work is the use of a 3.5 mm defect, where systemic reviews have concluded substantial evidence suggests a ≥ 5 mm defect could be considered of critical size in rats[53]. Use of a 3.5 mm defect allows for bilateral defects to be created so a therapeutic biomaterial and control site can be assessed in the same animal, reducing effects of genetic variability between animals, and thus requiring fewer animals in the study design. However, due to limited research in defects < 5 mm[7–9], further validation of a 3.5 mm calvarial defect is needed for application in a bilateral defect model, and to be considered of 'critical size'. Interestingly, in this work, the percent bone area filled of a 3.5 mm calvarial defect in healthy rats was 30 ± 24% at 12 weeks post-defect surgery (Figure 6). Further studies should be done with larger sized calvarial defect in ovariectomized animals at various time points following OVX surgery. Further validation of the short-term effects of OVX is needed for co-implementation with the critical sized calvarial defect models during this period of increased inflammation, remodeling activity, and differential ERα and ERβ expression caused by estrogen-deficiency.

In summary, the effect of estrogen deficiency on bone properties was found to be dependent on skeletal site and bone type, where OVX rats had decreased trabecular bone volume fraction in the tibia, increased tibial cortical area and calvarial bone volume, and no bone loss or gain in the mandible 14 weeks post-OVX. Additionally, enhanced bone healing was seen in the calvarial defect space of OVX rats compared to sham. Future studies should work to better understand the early effects of estrogen deficiency on cranial bone properties, as the co-implementation of the critical sized calvarial defect and OVX model is commonly used for the assessment of biomaterial implants for bone regeneration in osteoporotic conditions; researchers commonly implement a short OVX onset period prior to

calvarial defect creation (i.e., ≤ 6 weeks)[13,16–18] likely to minimize housing and experimental costs. The effect of OVX on calvarial healing may be dependent on the timing of defect creation relative to the onset of estrogen deficiency and is an important consideration for future studies wanting to represent the clinical scenario of cranial defects in postmenopausal osteoporotic women.

Ethics Approval

All animal experiments were completed in accordance with the NIH guide for the care of laboratory animals and with approval from the University of Massachusetts Institutional Animal Care and Use Committee (Protocol #3397).

Authors' Contributions

SD and AB designed the study. AB carried out the experiment, collected and led the analysis of data, and wrote the manuscript with the support of SD. JB assisted with carrying out the experiment. EM assisted in data analysis. SW assisted with experimental planning and contributed to the final version of the manuscript. SD supervised the project. All authors read and approved the final version of the manuscript.

Funding

This publication was supported by funding from NIH RO1 grant number 5RO1DE016523 and the Massachusetts Space Grant Consortium.

Acknowledgments

We thank Orla Gauvain and Molly Costa for their contributions to μCT analysis as well as Paige Ruschke and Riley Burnham for their assistance with calvarial defect procedures.

Graphics made with BioRender.com.

References.

1. Larsson S. Treatment of osteoporotic fractures. Scand J Surg 2002;91:140–6.
2. Yousefzadeh N, Kashfi K, Jeddi S, Ghasemi A. Ovariectomized rat model of osteoporosis: a practical guide. EXCLI J 2020;19:89–107.
3. Thompson DD, Simmons HA, Pirie CM, Ke HZ. FDA Guidelines and animal models for osteoporosis. Bone 1995;17:125S-133S.
4. Editor-Jennifer J. Westendorf. Osteoporosis: Methods and Protocols (Methods in Molecular Biology). Humana Press; 2008.
5. Lee JC, Volpicelli EJ. Bioinspired Collagen Scaffolds in Cranial Bone Regeneration: From Bedside to Bench. Adv Healthc Mater 2017;6.
6. Frieden T, Houry D, Baldwin G. Report to Congress: Traumatic Brain Injury in the United States 2015. https://www.cdc.gov/traumaticbraininjury/pubs/tbi_report_to_congress.html.
7. Spicer PP, Kretlow JD, Young S, Jansen JA, Kasper FK, Mikos AG. Evaluation of bone regeneration using the rat critical size calvarial defect. Nat Protoc 2012;7:1918–29.
8. Cooper GM, Mooney MP, Gosain AK, Campbell PG, Losee JE, Huard J. Testing the critical size in calvarial bone defects: revisiting the concept of a critical-size defect. Plast Reconstr Surg 2010;125:1685–92.
9. Schmitz JP, Hollinger JO. The critical size defect as an experimental model for craniomandibulofacial nonunions. Clin Orthop 1986:299–308.
10. de Almeida JM, Bosco AF, Faleiros PL, Pazmiño VFC, Murakawa AC, Bonfante S, et al. Effects of oestrogen deficiency and 17β-estradiol therapy on bone healing in calvarial critical size defects treated with bovine bone graft. Arch Oral Biol 2015;60:631–41.
11. Durão SFO, Gomes PS, Silva-Marques JM, Fonseca HRM, Carvalho JFC, Duarte JAR, et al. Bone regeneration in osteoporotic conditions: healing of subcritical-size calvarial defects in the ovariectomized rat. Int J Oral Maxillofac Implants 2012;27:1400–8.
12. Durão SF, Gomes PS, Colaço BJ, Silva JC, Fonseca HM, Duarte JR, et al. The biomaterial-mediated healing of critical size bone defects in the ovariectomized rat. Osteoporos Int J Establ Result Coop Eur Found Osteoporos Natl Osteoporos Found USA 2014;25:1535–45.
13. Develos Godoy DJ, Banlunara W, Jaroenporn S, Sangvanich P, Thunyakitpisal P. Collagen and mPCL-TCP scaffolds induced differential bone regeneration in ovary-intact and ovariectomized rats. Biomed Mater Eng 2018;29:389–99.
14. Dempster DW, Birchman R, Xu R, Lindsay R, Shen V. Temporal changes in cancellous bone structure of rats immediately after ovariectomy. Bone 1995;16:157–61.
15. Weng S-J, Yan D-Y, Tang J-H, Shen Z-J, Wu Z-Y, Xie Z-J, et al. Combined treatment with Cinnamaldehyde and β-TCP had an additive effect on bone formation and angiogenesis in critical size calvarial defect in ovariectomized rats. Biomed Pharmacother Biomedecine Pharmacother 2019;109:573–81.
16. Mardas N, Busetti J, de Figueiredo JAP, Mezzomo LA, Scarparo RK, Donos N. Guided bone regeneration in osteoporotic conditions following treatment with zoledronic acid. Clin Oral Implants Res 2017;28:362–71.
17. Chu M, Sun Z, Fan Z, Yu D, Mao Y, Guo Y. Bi-directional regulation functions of lanthanum-substituted layered double hydroxide nanohybrid scaffolds via activating osteogenesis and inhibiting osteoclastogenesis for osteoporotic bone regeneration. Theranostics 2021;11:6717–34.
18. Yang S, Wang L, Feng S, Yang Q, Yu B, Tu M. Enhanced bone formation by strontium modified calcium sulfate hemihydrate in ovariectomized rat critical-size calvarial defects. Biomed Mater Bristol Engl 2017;12:035004.
19. Zeng J, Guo J, Sun Z, Deng F, Ning C, Xie Y. Osteoblastic and anti-osteoclastic activities of strontium-substituted silicocarnotite ceramics: *In vitro* and *in vivo* studies. Bioact Mater 2020;5:435–46.

20. Pei M, Li J, McConda DB, Wen S, Clovis NB, Danley SS. A comparison of tissue engineering based repair of calvarial defects using adipose stem cells from normal and osteoporotic rats. Bone 2015;78:1–10.
21. Wronski TJ, Cintrón M, Dann LM. Temporal relationship between bone loss and increased bone turnover in ovariectomized rats. Calcif Tissue Int 1988;43:179–83.
22. Wronski TJ, Walsh CC, Ignaszewski LA. Histologic evidence for osteopenia and increased bone turnover in ovariectomized rats. Bone 1986;7:119–23.
23. Bouxsein ML, Boyd SK, Christiansen BA, Guldberg RE, Jepsen KJ, Müller R. Guidelines for assessment of bone microstructure in rodents using micro-computed tomography. J Bone Miner Res Off J Am Soc Bone Miner Res 2010;25:1468–86.
24. Morgan EF, Mason ZD, Chien KB, Pfeiffer AJ, Barnes GL, Einhorn TA, et al. Micro-computed tomography assessment of fracture healing: relationships among callus structure, composition, and mechanical function. Bone 2009;44:335–44.
25. Liu X, Bao C, Xu HHK, Pan J, Hu J, Wang P, et al. Osteoprotegerin gene-modified BMSCs with hydroxyapatite scaffold for treating critical-sized mandibular defects in ovariectomized osteoporotic rats. Acta Biomater 2016;42:378–88.
26. Tang Y, Tang W, Lin Y, Long J, Wang H, Liu L, et al. Combination of bone tissue engineering and BMP-2 gene transfection promotes bone healing in osteoporotic rats. Cell Biol Int 2008;32:1150–7.
27. Gielkens PFM, Schortinghuis J, De Jong JR, Raghoebar GM, Stegenga B, Bos RRM. Vivosorb®, Bio-Gide®, and Gore-Tex® as barrier membranes in rat mandibular defects: an evaluation by microradiography and micro-CT. Clin Oral Implants Res 2008;19:516–21.
28. Rosales Rocabado JM, Kaku M, Nozaki K, Ida T, Kitami M, Aoyagi Y, et al. A multi-factorial analysis of bone morphology and fracture strength of rat femur in response to ovariectomy. J Orthop Surg 2018;13:318.
29. Baldock PAJ, Need AG, Moore RJ, Durbridge TC, Morris HA. Discordance Between Bone Turnover and Bone Loss: Effects of Aging and Ovariectomy in the Rat. J Bone Miner Res 1999;14:1442–8.
30. Bagi CM, Mecham M, Weiss J, Miller SC. Comparative morphometric changes in rat cortical bone following ovariectomy and/or immobilization. Bone 1993;14:877–83.
31. Longo AB, Salmon PL, Ward WE. Comparison of *ex vivo* and *in vivo* micro-computed tomography of rat tibia at different scanning settings. J Orthop Res Off Publ Orthop Res Soc 2017;35:1690–8.
32. Liu J, Watanabe K, Dabdoub SM, Lee BS, Kim D-G. Site-specific characteristics of bone and progenitor cells in control and ovariectomized rats. Bone 2022;163:116501.
33. Levit M, Finn T, Sachadava S, Matsumura S, Shah J, Cantos A, et al. Menopause-Associated Changes in Mandibular Bone Microarchitecture Are Site-Specific. J Oral Maxillofac Surg 2024;82:485–93.
34. Goldberg S, Grynpas MD, Glogauer M. Heterogeneity of osteoclast activity and bone turnover in different skeletal sites. Arch Oral Biol 2016;71:134–43.
35. Allen MR, Burr DB. Chapter 4 - Bone Modeling and Remodeling. In: Burr DB, Allen MR, editors. Basic Appl. Bone Biol., San Diego: Academic Press; 2014, p. 75–90.
36. Westerlind KC, Wronski TJ, Ritman EL, Luo Z-P, An K-N, Bell NH, et al. Estrogen regulates the rate of bone turnover but bone balance in ovariectomized rats is modulated by prevailing mechanical strain. Proc Natl Acad Sci U S A 1997;94:4199–204.
37. Baldock PA, Morris HA, Need AG, Moore RJ, Durbridge TC. Variation in the short-term changes in bone cell activity in three regions of the distal femur immediately following ovariectomy. J Bone Miner Res Off J Am Soc Bone Miner Res 1998;13:1451–7.
38. Lane NE, Thompson JM, Haupt D, Kimmel DB, Modin G, Kinney JH. Acute Changes in Trabecular Bone Connectivity and Osteoclast Activity in the Ovariectomized Rat *In Vivo*. J Bone Miner Res 1998;13:229–36.
39. He Y-X, Zhang G, Pan X-H, Liu Z, Zheng L, Chan C-W, et al. Impaired bone healing pattern in mice with ovariectomy-induced osteoporosis: A drill-hole defect model. Bone 2011;48:1388–400.
40. Yamaura M, Nakamura T, Tsurukami H, Hijioka A, Narusawa K, Ohnishi H, et al. Local bone turnover in the metaphysis of the proximal tibia and the lumbar vertebra during the early periods after ovariectomy in rats. Calcif Tissue Int 1996;58:52–9.
41. Kennedy OD, Brennan O, Rackard SM, Staines A, O'Brien FJ, Taylor D, et al. Effects of ovariectomy on bone turnover, porosity, and biomechanical properties in ovine compact bone 12 months postsurgery. J Orthop Res 2009;27:303–9.
42. Bord S, Horner A, Beavan S, Compston J. Estrogen receptors alpha and beta are differentially expressed in developing human bone. J Clin Endocrinol Metab 2001;86:2309–14.
43. Khalid AB, Krum SA. Estrogen receptors alpha and beta in bone. Bone 2016;87:130–5.
44. Hall JM, McDonnell DP. The estrogen receptor beta-isoform (ERbeta) of the human estrogen receptor modulates ERalpha transcriptional activity and is a key regulator of the cellular response to estrogens and antiestrogens. Endocrinology 1999;140:5566–78.
45. Jee WS, Yao W. Overview: animal models of osteopenia and osteoporosis. J Musculoskelet Neuronal Interact 2001;1:193–207.
46. Li M, Shen Y, Wronski TJ. Time course of femoral neck osteopenia in ovariectomized rats. Bone 1997;20:55–61.
47. Wronski TJ, Dann LM, Horner SL. Time course of vertebral osteopenia in ovariectomized rats. Bone

1989;10:295–301.
48. Liu XL, Li CL, Lu WW, Cai WX, Zheng LW. Skeletal site-specific response to ovariectomy in a rat model: change in bone density and microarchitecture. Clin Oral Implants Res 2015;26:392–8.
49. Wang J, Li W, Xu S, Yang D, Wang Y, Lin M, et al. Osteoporosis influences the middle and late periods of fracture healing in a rat osteoporotic model. Chin J Traumatol Zhonghua Chuang Shang Za Zhi 2005;8:111–6.
50. Laib A, Kumer JL, Majumdar S, Lane NE. The Temporal Changes of Trabecular Architecture in Ovariectomized Rats Assessed by MicroCT. Osteoporos Int 2001;12:936–41.
51. Allison H, O'Sullivan LM, McNamara LM. Temporal changes in cortical microporosity during estrogen deficiency associated with perilacunar resorption and osteocyte apoptosis: A pilot study. Bone Rep 2022;16:101590.
52. O'Sullivan LM, Allison H, Parle EE, Schiavi J, McNamara LM. Secondary alterations in bone mineralisation and trabecular thickening occur after long-term estrogen deficiency in ovariectomised rat tibiae, which do not coincide with initial rapid bone loss. Osteoporos Int J Establ Result Coop Eur Found Osteoporos Natl Osteoporos Found USA 2020;31:587–99.
53. Vajgel A, Mardas N, Farias BC, Petrie A, Cimões R, Donos N. A systematic review on the critical size defect model. Clin Oral Implants Res 2014;25:879–93.

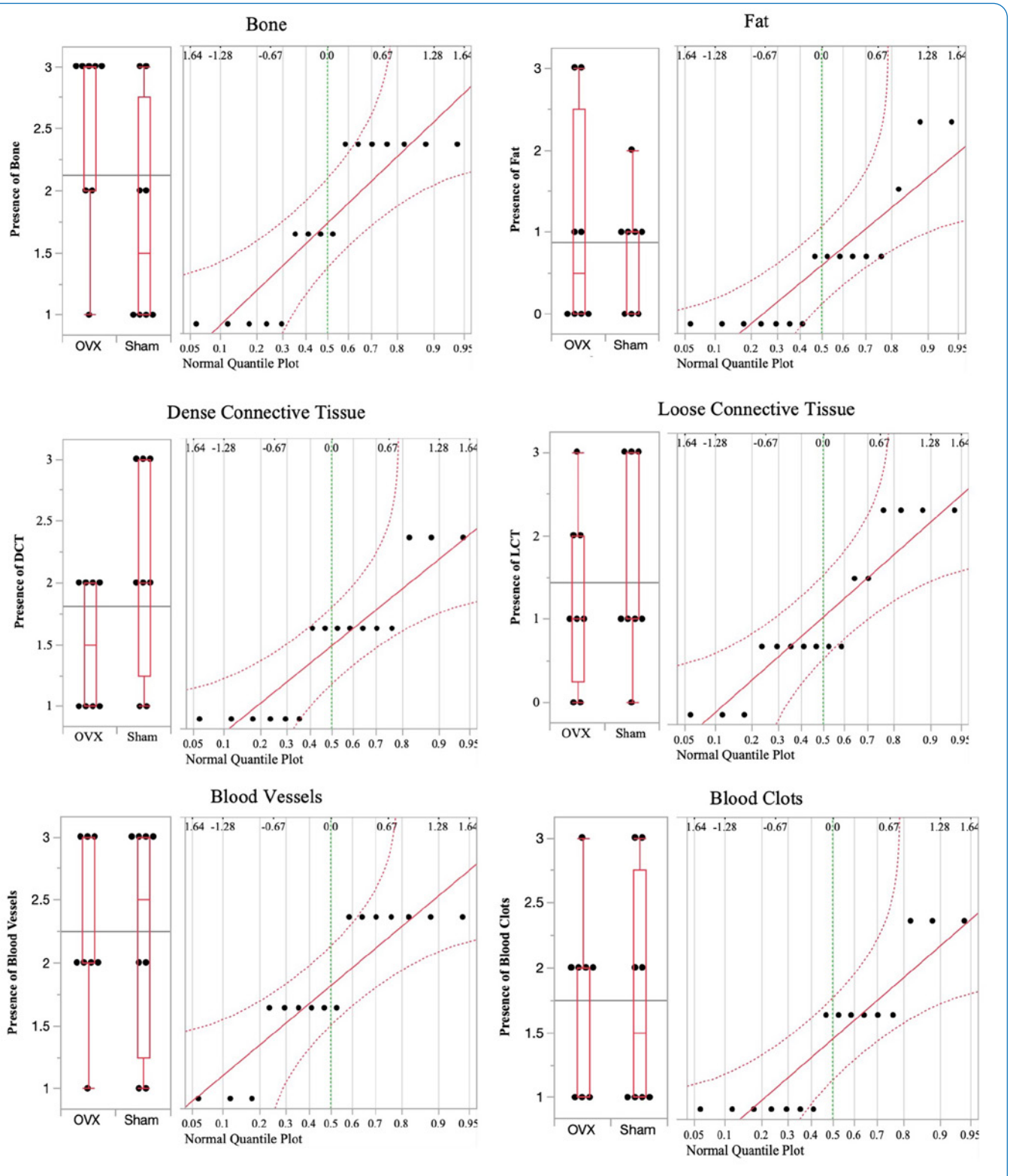

Figure S1. Normality assessment of histology grading results for tissue types (bone, fat, dense CT, loose CT, blood vessels, and blood clots) including per-metric distribution (weighted by group) and normal quantile plots (pooled).

Table S1. Pairwise effect size and 95% CI for longitudinal μCT parameters of calvarial defect healing (% bone volume filled and % TMD).

Calvarial Defect Space: % Bone Volume Filled							
Effect	**Comparison (Level)**		**Value Diff.**	**Cohen's d Effect Size**	**Cohen's d Lower CI**	**Cohen's d Upper CI**	**P-Value**
Group	OVX	Sham	28.25	1.63	1.00	2.25	< 0.001
Time Point	Week 4	Week 8	10.68	0.62	-0.05	1.28	0.070
	Week 8	Week 12	6.02	0.35	-0.31	1.00	0.302
	Week 4	Week 12	16.70	0.97	0.28	1.64	0.006
Group * Time Point	OVX, Week 4	OVX, Week 8	13.27	0.77	-0.17	1.70	0.110
	OVX, Week 8	OVX, Week 12	9.42	0.54	-0.39	1.47	0.254
	OVX, Week 4	OVX, Week 12	22.69	1.31	0.34	2.26	0.008
	OVX, Week 4	Sham, Week 4	22.53	1.30	0.34	2.26	0.008
	Sham, Week 4	Sham, Week 8	8.08	0.47	-0.46	1.39	0.327
	Sham, Week 8	OVX, Week 8	27.71	1.60	0.62	2.57	< 0.001
	Sham Week 8	Sham, Week 12	2.63	0.15	-0.77	1.08	0.663
	Sham, Week 4	Sham, Week 12	10.71	0.62	-0.32	1.55	0.195
	Sham, Week 12	OVX, Week 12	34.50	1.99	0.98	2.99	< 0.001
Calvarial Defect Space: % TMD							
Group	OVX	Sham	0.55	0.12	-0.42	0.65	0.789
Time Point	Week 4	Week 8	7.84	1.65	0.91	2.37	< 0.001
	Week 8	Week 12	12.09	0.89	0.21	1.57	0.010
	Week 4	Week 12	12.09	2.54	1.71	3.36	< 0.001
Group * Time Point	OVX, Week 4	OVX, Week 8	7.80	1.64	0.65	2.61	0.001
	OVX, Week 8	OVX, Week 12	4.92	1.03	0.08	1.97	0.033
	OVX, Week 4	OVX, Week 12	12.71	2.67	1.59	3.73	< 0.001
	OVX, Week 4	Sham, Week 4	0.17	0.04	-0.89	0.96	0.941
	Sham, Week 4	Sham, Week 8	7.88	1.66	0.67	2.63	0.001
	Sham, Week 8	OVX, Week 8	0.08	0.02	-0.91	0.94	0.971
	Sham Week 8	Sham, Week 12	3.59	0.76	-0.18	1.69	0.116
	Sham, Week 4	Sham, Week 12	11.48	2.41	1.36	3.44	< 0.001
	Sham, Week 12	OVX, Week 12	1.40	0.30	-0.63	1.22	0.534